



# Performance evaluation of microbial fuel cell fabricated using green nano-graphene oxide as coating anode material

Afaf Abdel Razik Mohamed<sup>1</sup> · Ali El-Dissouky Ali<sup>1</sup> · Mohamed Salah El-Din Hassouna<sup>2</sup> · Amel F. Elhusseiny<sup>1</sup> · Abd El-Hady B. Kashyout<sup>3</sup> · Zhen He<sup>4</sup> · Hanan Moustafa<sup>2</sup>

Received: 21 August 2023 / Revised: 27 September 2023 / Accepted: 1 October 2023  
© The Author(s) 2023, corrected publication 2024

## Abstract

A dual-chamber microbial fuel cell (MFC) was fabricated and optimized for electricity generation. Titanium wire, graphite rod, and carbon cloth supported on stainless steel mesh were the best current collector, anode, and cathode electrode materials, respectively. To enhance the efficacy of the system, carbon-based materials in nano-scale (nanocarbonized materials) were prepared from pomegranate peel waste at different hydrothermal temperatures (300, 500, and 700 °C), and were used as anode coating material. The synthesized coating materials were characterized using EDX, FT-IR, Raman spectroscopy, XRD, TEM, fluorescence, UV, and XPS analyses. Data showed that nanocarbonized material prepared at 500 °C exhibited high surface area (682 m<sup>2</sup>/g), high pore size (122 nm), and indicated the presence of graphene oxide (GO) structure. The electrochemical behavior of MFC was monitored by cyclic voltammetry and impedance measurements. Results revealed that the anode coated with GO provided high MFC performance with a maximum voltage of around 1000 mV, and a maximum current of 0.1 mA, corresponding to a maximum power density of 12.46 W/m<sup>2</sup>, which is 2.85-fold higher than that of a cell with a free graphite plate as an anode. Furthermore, the large charge transfer resistance and the low diffusive resistance observed upon coating the anode demonstrated the anode is functioning as a capacitor. The reported results proposed graphene oxide prepared from pomegranate peels as a novel coating anode material prepared from waste sustaining the idea of green curricular economy

**Keywords** Microbial fuel cell performance · Anode · Nanocarbonized materials · Graphene oxide · Pomegranate peels

## 1 Introduction

Bio-electrochemical systems (BESs) are important techniques that have gained a lot of interest for energy and wastewater treatment. BESs are bioreactors that use bacteria as catalysts to generate electricity directly from organics

in wastewater, thereby incorporating green technology [1]. Microbial fuel cell (MFC) is one of the BESs, acting as an eco-friendly bio-electrochemical technology with promising qualities for a sustainable and green future. There are numerous MFC types that can be categorized according to their design or mode of operation [2].

The concept of MFC operation involves an anode and a cathode which may or may not be separated by a semi permeable membrane. In order to metabolize the substrate (waste stream) and produce protons that will flow through a proton exchange membrane to the cathode chamber and give electrons to the cathode through an external wire, the bacteria are typically cultured at the anode in an anaerobic environment [3, 4]. Once they get to the cathode, the resultant electrons from the anode chamber will combine with oxygen, which will operate as an electron acceptor in the presence of protons, to form water as a byproduct [5]. As a result, MFC can be viewed as a sustainable water treatment method because it generates water as a byproduct.

✉ Hanan Moustafa  
Hanan.abdallah@alexu.edu.eg

<sup>1</sup> Chemistry Department, Faculty of Science, Alexandria University, 2 Bagdad Street, PO Box 2-Moharrem Beck, Alexandria 21321, Egypt

<sup>2</sup> Institute of Graduate Studies and Research, Alexandria University, Alexandria 21526, Egypt

<sup>3</sup> Electronic Materials Department, City of Scientific Research and Technological Applications (SRTA-City), SRTA, Egypt

<sup>4</sup> Department of Energy, Environmental and Chemical Engineering, Washington University in St. Louis, St. Louis, MO 63130, USA

Microbial inoculums, the chemical substrate in the waste, the proton exchange membrane (PEM), and the electrode material are some of the variables that might determine how well MFCs operate. As it controls bacterial growth, the rate at which organic matter and pollutants are removed from the system, and the generation and transformation of electrons into the cathode compartment, the anode is one of the important variables impacting the performance of MFCs and their potential for commercialization. The anode materials must have high conductivity, good biocompatibility, strong thermal and mechanical stability, high chemical stability, and a large surface area in order to meet high-performance requirements. Additionally, there are still many obstacles to overcome for the best design of anode materials to improve the performance of MFCs, including the inoculation of microorganisms onto electrode surfaces, the sustainability of microbes in the electrode environment, the electron transfer rate for extended power generation, and the longevity of MFCs [6].

Different electrode materials have been developed to increase the rate of pollution removal and energy production efficiency. Although carbon-based nanomaterials such as glassy carbon, nanofiber, carbon felt, carbon cloth, nanorods, flexible sheets, and meshes were employed as anodes, their expensive costs prevented them from being used on larger scales [7]. As anodes, composite materials, metals, metal oxides, conductive polymer-based materials, and derivatives of graphene were also employed. Making bio-based materials is essential in the modern world. Despite the fact that conventional materials are commonly used as anode materials in MFC applications, one common drawback is the addition of additional costs, and mediocre performance, and its preparation has certain environmental challenges [8]. The option of using a readily available, low-cost material is a really intriguing bonus in this situation. Anodes made from biomass waste such as sugar cane [9], coffee-based anode [10], onion peels [11], and coconut shell [12] are being considered an alternative to conventional electrode materials, because they are readily available, affordable, and capable of removing environmental contaminants brought on by the direct burning of waste biomass. These materials can also produce electricity and enhance the functionality of MFCs [13, 14].

The basic physical and chemical characteristics of carbon materials made from biomass, such as activated carbon, reduced graphene oxide, graphene oxide, and nanofibers, include heat resistance, high conductivity, and high thermal conductivity. Because of their high conductivity and high porosity in their structure, they were employed as an adsorbent to remove pollutants or in the fabrication of electrodes for MFCs. They are also cheap and renewable because they are created from waste biomass [15]. Consequently, one of the objectives of the present MFC technology research is

to create more affordable, environmentally friendly, and electrochemically stable electrode anodes by coating regular graphite plate with carbon-based material in nano-scale (nanocarbonized material) extracted from pomegranate peels. Pomegranate peels contain bioactive chemicals that are abundant in oxygen groups, which promote the rapid growth of bacteria [16]. To the best of our knowledge, pomegranate peels have never been used as biomass waste in the production of anodes for MFCs. Here, materials made from pomegranate peels that were then carbonized at nano-scale were created at hydrothermal temperatures of 300, 500, and 700 °C while containing ferrocene as a catalyst. These materials will be employed as anode coating materials in the constructed double-chamber MFC to increase power production.

Utilizing EDX, FT-IR, Raman, XRD, TEM, fluorescence, UV, surface area, and XPS analyses, the synthesized nanocarbonized materials were thoroughly characterized. With different current collectors and electrode materials used in the anode and cathode chambers, the operating parameters for the production of bioelectricity were optimized. Evaluations have been performed of the MFC's performance and electrochemical behavior using cyclic voltammetry and impedance. Additionally, pomegranate peel hydrolysate and untreated pomegranate peels were both used to test the constructed MFC's performance for comparison purposes.

## 2 Experimental work

### 2.1 Synthesis and characterization of pomegranate peels and nanocarbonized material prepared from pomegranate peels

The pomegranate fruits were purchased from the local fruit market, and the peels were manually removed. The collected peels were cleaned, dried at 60°C for 6 h, then crushed and ground for 5 min in a ball mill (FRITSH, pulverisette 7) to pass through sieves with a mesh size of 20. Energy dispersive X-ray analysis (EDX), thermal gravimetric analysis (TGA), Fourier transform infrared analysis (FT-IR), Raman spectroscopy, and X-ray diffraction (XRD) were used to characterize the dried pomegranate peel powder that resulted. In accordance with the findings of the thermal gravimetric study of the powdered pomegranate peels, three distinct hydrothermal temperatures (300 °C, 500 °C, and 700 °C) were chosen for the manufacture of the nanocarbonized material. One gram of the characterized powder was used as the precursor for the creation of nanocarbonized materials (black in color) according to Asnawi et al. method [17], where the preparation was carried out at different hydrothermal temperatures of 300°C, 500°C, and 700°C using a muffle furnace [18, 19] in presence of 0.2 g ferrocene as a catalyst. Utilizing EDX, FT-IR, Raman spectroscopy, XRD,

TEM, fluorescence UV, surface area, and X-ray photoelectron spectroscopy (XPS) examination, the generated nanocarbonized material was also thoroughly characterized. Infrared spectra (KBr pellets, 3-mm thickness) were recorded on a Perkin-Elmer Infrared Spectrophotometer (FTIR 1650). Electronic absorption spectra were recorded in the 200–600 nm region in UV-vis evolution 300 spectrophotometer equipped with quartz cells of 1.0-cm path length. Fluorescence measurements were recorded on Parkin-Elmer LS-55 fluorescence spectrometer, using quartz cuvettes of 1.0-cm path, within the wavelength range 380–600 nm at room temperature ( $25 \pm 1^\circ\text{C}$ ). The surface morphology of prepared nanocarbonized materials was determined by using transmission electron microscopy (TEM) JICA (J 11-0254) model. Thermal analysis was measured in the temperature range from 50 to  $800^\circ\text{C}$  in a stream of nitrogen atmosphere by a Linseis Sta Pt1000 thermal analyzer. The specific surface area was estimated by sears' method [20] and the pore volume of the three nanocarbonized materials was determined from the nitrogen adsorption isotherms at 77 K using the Brunauer-Emmett-Teller (BET) equation and the BELSORP-miniX (S/N: 149, Version 1.0.9.0) instrument. The total pore size was estimated to be the liquid volume of the adsorbate ( $\text{N}_2$ ) at a relative pressure of 0.99. The surface area was estimated by agitating 1.5 g of the sample in 100 ml of diluted hydrochloric acid (0.1 N) at  $\text{pH}=3$ . Then add 30 g of sodium chloride while the suspension was stirring and then the volume of the solution was adapted to 150 mL by ionized water. This solution was titrated against sodium hydroxide (0.1 N) to

raise pH from 4 to 9 and the volume is recorded. Summary of pomegranate peels and nanocarbonized material preparation and characterization is shown in Fig. 1.

## 2.2 Synthesis of pomegranate peel hydrolysate

The pomegranate peels were hydrolyzed by acid according to the reported method [21], whereas pomegranate peels were acid hydrolyzed using sulfuric acid (Aldrich) at a 1:10 ratio at  $100^\circ\text{C}$  for 30 min before being filtered and neutralized with NaOH.

## 2.3 Coating the anode electrode with the nanocarbonized material

After characterization of the prepared nanocarbonized materials, a certain amount (0.3 gm) was used for 10% coating. Coating was carried out according to the reported method [22]. It is based on using polyvinylidene difluoride (PVDF) dissolved in N-methyl 1,2 pyrrolidone (NMP) as a binder. The binder solution was prepared by dissolving 0.32 g of PVDF in 16 ml of NMP. To prepare a 10% coating, 0.03 g of the characterized nanocarbonized material was added to 150  $\mu\text{l}$  of the prepared binder solution, followed by sonication for 5 min. Before coating, the graphite plate (anode electrode) was cleaned with acetone, followed by drying at  $70^\circ\text{C}$  for 30 min. Finally, a brush was used to coat the anode with the prepared 10% coating of nanocarbonized material. MFC performance was also evaluated using either untreated

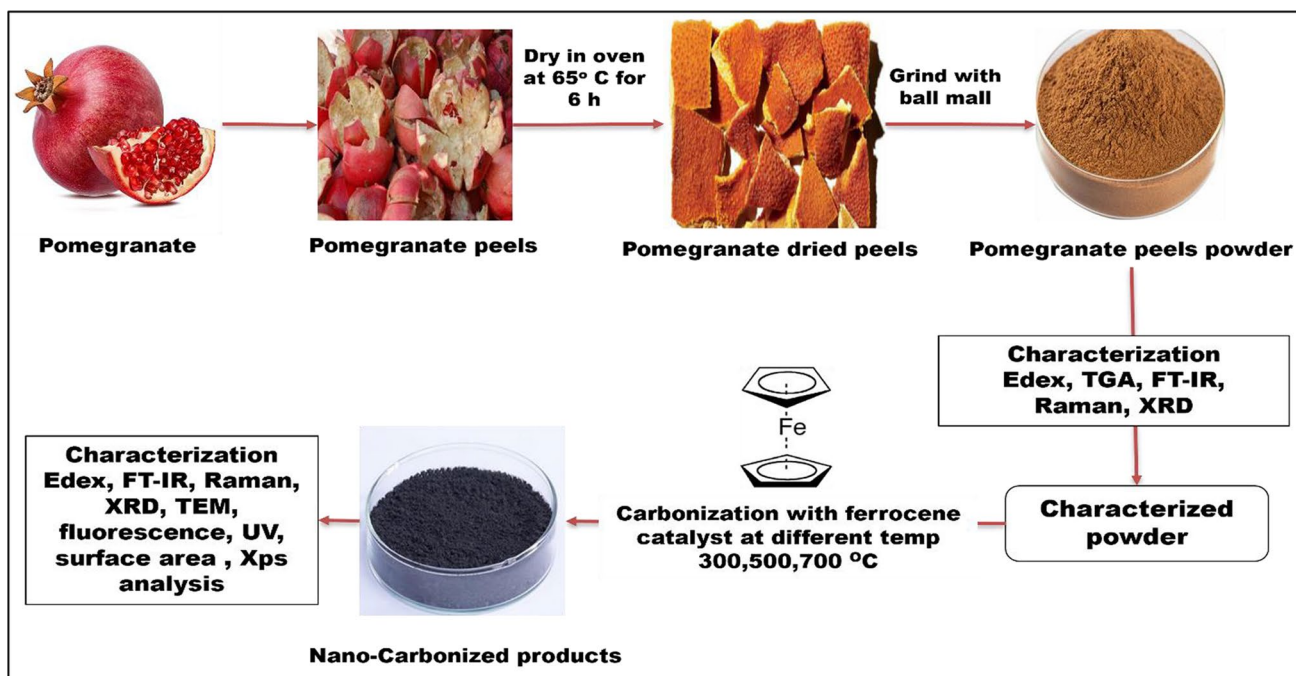


Fig. 1 Preparation and characterization of nanocarbonized materials at different hydrothermal temperatures from pomegranate peels

pomegranate peels and pomegranate peel hydrolysate as substrate to test the importance of coating anode of MFC with nanocarbonized materials extracted from pomegranate peels over using it as substrate with simple or without any treatment.

## 2.4 Construction of MFC bioreactor

The constructed dual chamber MFC bioreactor used in this study is shown in Fig. 2; the bioreactor is made of neoprene rubber sheets along with acrylic sheets. In all experiments, anode and cathode chambers are separated by a cation exchange membrane (CEM; NAFION 117). The anodic chamber contains organic matter that is metabolized by microorganisms for growth and energy production while generating protons and electrons. The anolyte was prepared using synthetic media [23] consisting of 1 g/L  $\text{CH}_3\text{COONa}$ , 15 g/L  $\text{NH}_4\text{Cl}$ , 50 g/L  $\text{NaCl}$ , 2 g/L  $\text{CaCl}_2$ , 1.5 g/L  $\text{MgSO}_4$ , 10 g/L  $\text{NaHCO}_3$ , and 1 ml/L trace elements. The cathode chamber contains 100 mM potassium dichromate in 250 mM sulfuric acid as catholyte. It is worth mentioning that acidified potassium dichromate was used as electron acceptor instead of oxygen, which is cheaper and easier to handle, but previous studies reported that, using dissolved oxygen has been shown to be proportional to the concentration of the dissolved oxygen in the catholyte, which is limited in itself by the solubility of oxygen in water as well as by the extraneous energy requirement for the exogenous supply of oxygen [24, 25]. Accordingly, substituting oxygen with other electron acceptors such as potassium dichromate can provide relatively faster rates of reduction and a higher theoretical redox potential [24, 26]. The distance between the anode and cathode electrodes was approximately 4 cm. Anaerobic sludge used in this study was provided by Alexandria East Sewage Treatment Plant and was used to inoculate 120 mL anolyte in the anode chamber of the MFC after activation and cultivation. The electrodes were connected by an external resistance (R) varying from 10000 to 10  $\Omega$ . All

experiments were carried out at  $37 \pm 2^\circ\text{C}$ . The MFC voltage and current were measured daily using a multimeter (model: CHY DT-9205A+).

## 2.5 Optimizing the operating conditions

The execution of a series of tests is provided below with the aim of optimizing the operating conditions for bioelectricity generation:

### 2.5.1 Current collectors

Different experimental trials were carried out using various current collectors to connect anode and cathode electrodes externally; for example, copper wire of 1-mm diameter connected both electrodes; copper wire of 1-mm diameter was connected to the anode, while titanium wire of 1-mm diameter was connected to the cathode; and finally, both electrodes were connected to titanium wire of 1-mm diameter.

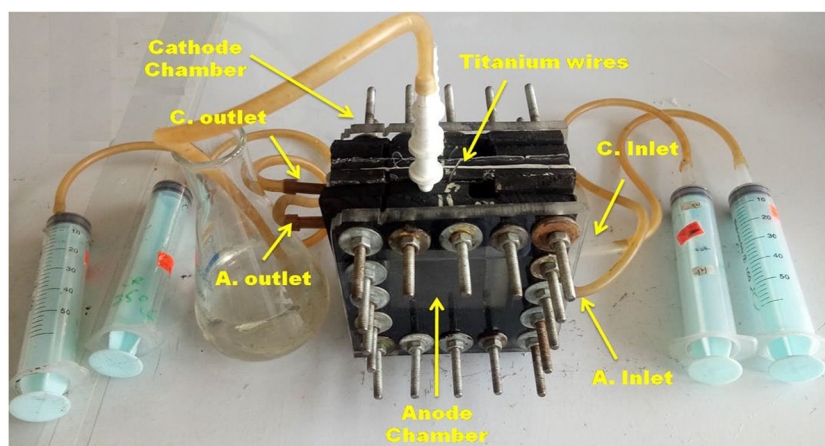
### 2.5.2 Electrode material

Different anode and cathode electrodes were used where titanium wire of 1-mm diameter served as the current collector in each trial, for example (both electrodes are carbon cloth supported on stainless steel mesh); graphite plate was the anode and carbon cloth supported on stainless steel mesh was the cathode and both electrodes are graphite plate.

## 2.6 Electrochemical characterization

The electrochemical characterization of the compact dual-chamber MFCs was carried out after the system started up successfully and at a stable reaction condition (at steady state). Polarization is the common and best method to evaluate MFC performance, but in this study, cyclic voltammetry (CV) using an Origa Flex Potentiostat (a modular and vertical multichannel made in Know-How and originally

**Fig. 2** Constructed dual chamber microbial fuel cell



manufactured in France) was utilized for the description of the electrochemical behavior. In cyclic voltammetry and electrochemical impedance spectroscopy, measurements were carried out for the anode, the cathode, and the MFC in a frequency range of 100 kHz to 0.01 mHz with an ac signal of 10-mV amplitude. Anode impedance spectra were recorded using the anode (graphite plate) as the working electrode (7 cm×1 cm×0.5 cm) and the cathode carbon cloth supported on stainless steel mesh as the counter electrode (5 cm×5 cm). During these measurements, the Ag/AgCl (Hanna instrument) reference electrode in the anode chamber was used as the reference electrode. When Executive Information Systems (EIS) electrochemical impedance spectroscopy measurements were performed for the MFC at several applied cell voltages, the anode was used as the working electrode and the cathode was used as the reference. Since the scan rate of the experiment controls how fast the applied potential is scanned, cyclic voltammetry was carried out at different scanning rates (10, 25, 50, and 100 mV/s) (based on the recommended scanning rate from zero to 100 mV/s) [27, 28]. All measurements were carried out at atmospheric pressure and room temperature with a frequency of 0.01 Hz–100 MHz and a voltage of 0 to 1000 mV. For data acquisition, OrigaMaster 5 was used. Specific capacitance was calculated using the following Eq. (1)

$$cp = a/[2mk(v_2 - v_1)] \quad (1)$$

where  $C_p$  is the specific capacitance in F/g.  $a$  is the area inside the CV curve having unit AV.  $m$  is the mass of active material.  $K$  is the scan rate of CV in volts per second and  $V_2-V_1$  is the potential window of CV (total voltage range).

## 3 Results and discussion

### 3.1 Characterization of pomegranate peels and nanocarbonized materials

The pomegranate peels and the prepared nanocarbonized materials were fully characterized using EDX, FT-IR, Raman, XRD, TEM, fluorescence UV, surface area, and XPS analysis. The analysis of pomegranate peels and nanocarbonized materials at different hydrothermal temperatures is given in Table 1.

The surface area of pomegranate peels and produced nanocarbonized materials at different temperatures was measured by rapid method (sears' method) according to the following Eq. (2):

$$S(m^2/g) = 32 V - 25 \quad (2)$$

where  $V$  is sodium hydroxide volume required to raise the pH of the tested sample from 4 to 9. The obtained results

show that nanocarbonized material at 500°C showed much higher surface area ( $\approx 682 \text{ m}^2 \text{ g}^{-1}$ ) with respect to the other nanocarbonized materials with highest distribution of pore size (122 nm) and using of these two nanocarbonized materials at 500 and 700 °C are promising as coating material for anodes in MFC as enhancement bacteria growth [29].

Table S1 shows the chemical composition of pomegranate peels and nanocarbonized material prepared at 500°C; besides, Fig. S1 showed their EDX analysis. The obtained results suggested that a reduction reaction took place by hydrothermal process and ferrocene used only as a catalyst. Figure 3 A displays the thermogravimetry analysis (TGA) of pomegranate peels. As shown, the decomposition process of pomegranate peels started at 150°C and the material was reduced by increasing temperature, which may be due to the decomposition of organic components such as hemicellulose, and cellulose [30]. Therefore, the hydrothermal process of pomegranate peels will be processed at different temperatures 300°C, 500°C, and 700°C to prepare nanocarbonized materials. Chemical functional groups of pomegranate peels and different nanocarbonized materials were identified by FTIR analysis. Figure 3 B shows the pomegranate peel spectrum, which confirmed the complex nature of the peels and proved the presence of a wide variety of compounds. The spectra showed a long bandwidth at  $3403 \text{ cm}^{-1}$  corresponding to the O–H stretching band, confirming the presence of phenolic acids. The C–H stretching band of the alkane group was detected at a bandwidth of  $2936 \text{ cm}^{-1}$ . The sharp mid-intense peak at  $1729 \text{ cm}^{-1}$  attributed to the carbonyl group C=O, indicating the presence of ketones, aldehydes, and carboxylic acids. The moderately sharp peak at  $1624 \text{ cm}^{-1}$  was assigned to unsaturated compounds (alkenes). The  $\text{CH}_2$  bending appeared at  $1348 \text{ cm}^{-1}$  suggesting the presence of cellulose. However, the peak at  $1231 \text{ cm}^{-1}$  was assigned to  $-\text{CH}_3\text{CO}$  stretching, confirming the presence of ethers. The peak that appeared at  $874 \text{ cm}^{-1}$  may correspond to  $-\text{CCH}$  and  $-\text{COH}$  bending [31]. Thus, pomegranate peels are rich in oxygenated surface groups. The FT-IR spectra of nanocarbonized materials prepared at different hydrothermal temperatures showed the low existence of some wave number bands ( $589, 874, 1056, 1231,$  and  $1348 \text{ cm}^{-1}$ ) indicating a reaction between pomegranate peels and ferrocene. The formation of new bands at  $2352\text{--}2359 \text{ cm}^{-1}$  was assigned to C–O stretching; other bands appeared at  $1542\text{--}1547 \text{ cm}^{-1}$  and corresponded to the presence of the C=C group, indicating that the reduction process took place. The existence of the C–O group might be beneficial for the use of these nanocarbonized materials as electrodes to improve the growth of bacteria [30]. X-ray diffraction (XRD) of pomegranate peels and nanocarbonized materials is illustrated in Fig. 3C to investigate the crystal structure and phase information. The XRD pattern of the pomegranate peels displayed a broad diffraction peak at  $2\theta = 21.73^\circ$ ,

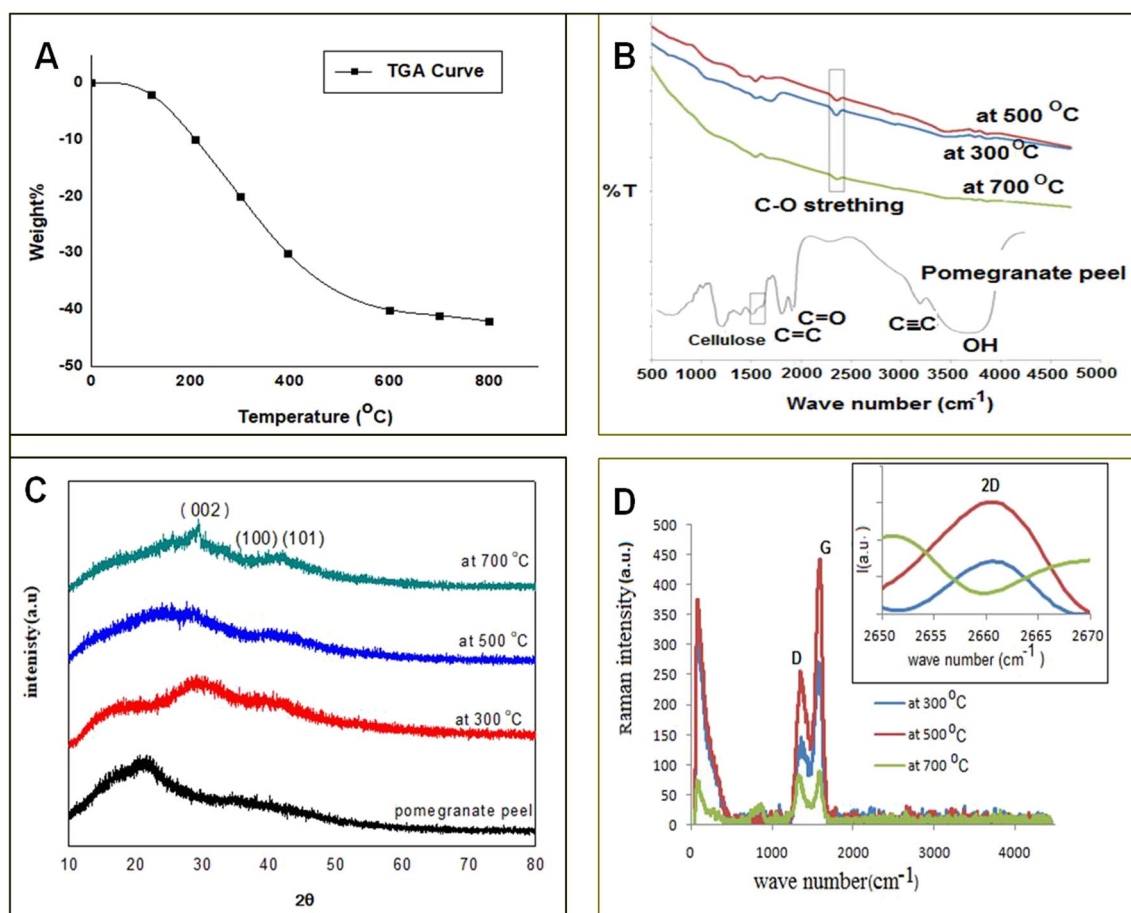


**Fig. 3** Characterization of pomegranate peels and nanocarbonized materials prepared at different temperatures; **A** TG analysis of pomegranate peels, **B** FT-IR spectra, **C** XRD pattern, and **D** Raman spectra

**Table 1** Analysis of pomegranate peels and nanocarbonized materials

	Ash wt%	Moisture wt%	yield%	Specific surface area m <sup>2</sup> /g	Pore size, nm
Pomegranate peels powder	2.75	9.78		10.2	
Nanocarbonized material at 300°C			50	23	27.006
Nanocarbonized material at 500°C			32	682.2	122.31
Nanocarbonized material at 700°C			27	570.2	24.613

indicating the complex nature of the precursor material and the appearance of cellulose compounds. The broad peak was shifted to a higher diffraction angle, and the peak became sharper with increasing the temperature of the carbonization process. This was confirmed by the appearance of the diffraction line C (002) at  $2\theta = 26^\circ$ . The nanocarbonized material showed a broad peak around  $2\theta = 41.73^\circ$  which may be due to the overlapping of (100) and (101) planes (ICDD card no. 00-001-0640), which originated from the hybridization of  $sp^2$  carbons, which is called turbostratic structure [32]. The spectrum of the hydrothermal process of

the raw material (pomegranate peels) at 300°C displayed  $2\theta$  at  $17.82^\circ$  indicating formation of fewer graphene oxide (GO) structures due to an uncompleted carbonization process. Moreover, by increasing the temperature than 300°C, the  $2\theta = 17.82^\circ$  disappeared, revealing chemical reduction, forming a more regular multilayer graphene-like structure, which may be reduced graphene oxide (rGO) [33, 34]. Raman spectroscopy enables the observation of edges, doping, flaws, strain, disorder, and chemical alterations in any material. Furthermore, Raman spectroscopy is useful for confirming the presence of  $sp^2$  phase. In Fig. 3D, there are two peaks for

both the G and D bands at  $1588\text{ cm}^{-1}$  and  $1345\text{ cm}^{-1}$ , respectively, which are detected for the carbon surface. These peaks may indicate the presence of the graphitic crystalline structure, which originated from the stretching vibration of the  $\text{sp}^3/\text{sp}^2$  orbitals of the carbon atom on both the hexagonal aromatic sheet and the lattice disordering [35].  $I_D/I_G$  is an intensity ratio for the measurement of the zone edges of graphitic clusters as  $D/G$  ratio is related to  $\text{sp}^3/\text{sp}^2$  carbon ratio. A decrease in this ratio improves the ordered regions of the cluster sizes in a complete  $\text{sp}^2$  network with fewer vacancies or disorder defects [36]. This ratio has the order nanocarbons at  $700\text{ }^\circ\text{C}$  ( $0.88$ ) >  $500\text{ }^\circ\text{C}$  ( $0.57$ ) >  $300\text{ }^\circ\text{C}$  ( $0.54$ ), which suggests an increase in the graphitic crystallinity  $\text{sp}^2$  of carbon and a decrease in disordering with an increase in temperature [36, 37]. The spectra of nanocarbons prepared at  $300$  and  $500\text{ }^\circ\text{C}$  displayed the presence of 2D at  $\approx 2660.50\text{ cm}^{-1}$  revealing the absence of any defects and the formation of **GO structure**. However, this band disappeared with increasing the temperature of carbonization, conforming to the formation of rGO.

The surface morphology of nanocarbons was examined by TEM micrograph, as shown in Fig. 4. Irregular shape and unorganized particle size were caused by cracking of the structure of nanocarbons prepared at  $300\text{ }^\circ\text{C}$  due to its instability under a high-energy beam. In contrast, nanocarbons prepared at  $500\text{ }^\circ\text{C}$  and

$700\text{ }^\circ\text{C}$  showed higher stability under a high-energy electron beam, which released a transparent reduced graphene oxide/graphene nanofiber hybrid structure that may lead to the formation of rGO nanosheets with dimensions >  $500\text{ nm}$ . HRTEM images in the bottom images show a high order of fringes with the value of  $d$ -spacing =  $0.225\text{ nm}$  [35]. Also, the selected area electron diffraction shows the spots of planes (002) and (100) of the graphene oxide structure as shown in the sample prepared at  $500\text{ }^\circ\text{C}$ . This result is confirmed by Raman spectroscopy studies as an exciting 2D band at  $2660.50\text{ cm}^{-1}$  [38, 39]. Therefore, by linking the results of morphology, Raman spectroscopy, and structural properties (XRD), it is proved that there is a low existence or lack of oxygen functionality in the structure of graphene composition with increasing the temperature of the hydrothermal process.

In Fig. S2, the oxygen-containing functional groups, such as epoxy (C–O–C), carboxyl groups (COOH), and hydroxyl groups (COH), lead to the overlap of many fluorescence peaks resulting from its electronic energy transitions. Thus, increasing the hydrothermal temperature is accompanied by a decrease in the fluorescence intensity with a slightly blue shift in the band position, suggesting a zero-band gap and no fluorescence characteristics. These results are consistent with XRD analysis of rGO formation at elevated temperatures [40]. The UV-visible spectra of the nanocarbons

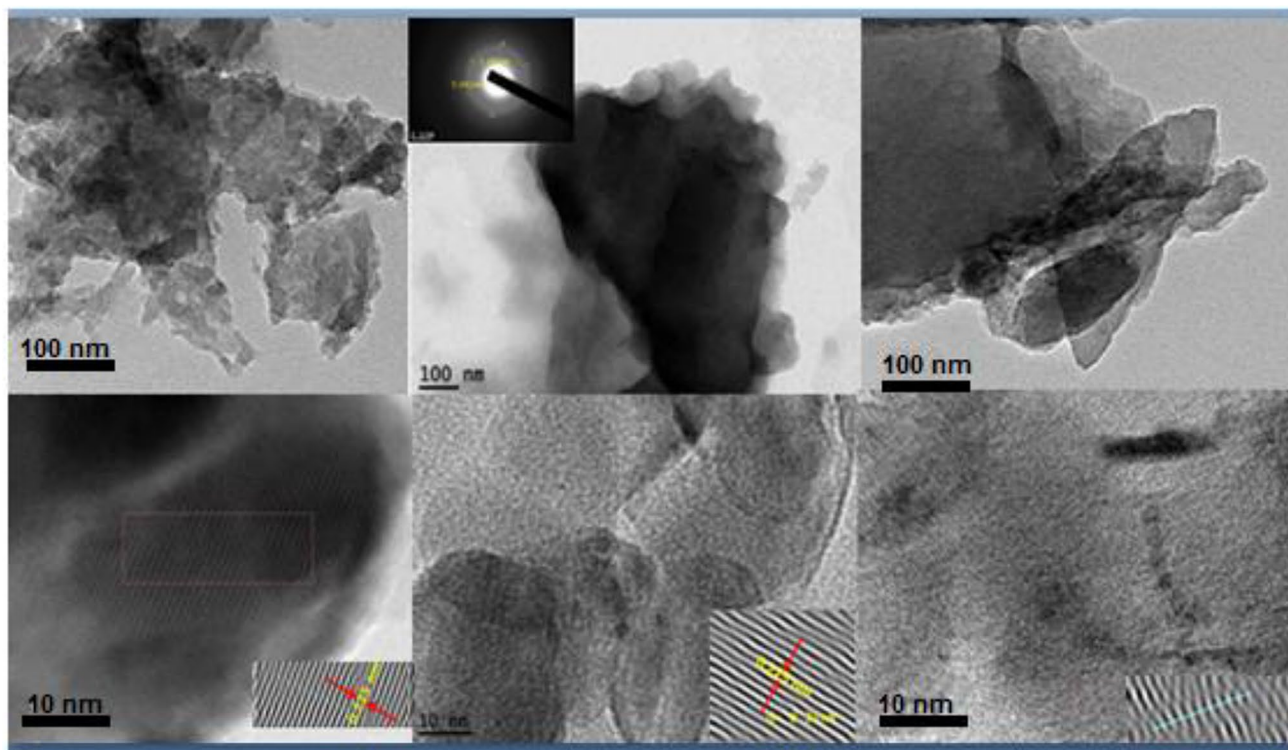


**Fig. 4** TEM images of nanocarbons prepared at **a**  $300\text{ }^\circ\text{C}$  (left), **b** at  $500\text{ }^\circ\text{C}$  (middle), **c** at  $700\text{ }^\circ\text{C}$  (right)

materials prepared at different temperatures are shown in Fig. S3. The spectra exhibited one band centered at 220–230 nm attributed to  $\pi$ - $\pi^*$  transitions of aromatic C=C bonds, and a shoulder centered at 260–270 nm appear at a hydrothermal process of 500°C corresponding to  $n$ - $\pi^*$  transitions of CHO bonds of GO structure [41]. Figure 5 presents the XPS spectra of the nanocarbons assembled by GO and rGO nanosheets. The C<sub>1s</sub> peaks of nanosheet GO appear at 284, 286, 287, and 288 eV, which were assigned to C–C, C–OH, C=O, and O–C=O, respectively [42]. Increasing temperature led to an increasing C/O ratio where the reduction process occurs and rGO is formed; the C<sub>1s</sub>/O<sub>1s</sub> ratios of GO and rGO were 1.2 and 1.6, respectively. This outcome supports the considerable GO reduction with increasing temperature. In the GO structure, the presence of the function groups enhances the conductivity of the nanosheets and makes them readily applicable as electrodes. Based on these results and data, the prepared GO as nanocarbons prepared at 500°C is selected to be used as the electrode coating material. The peak fitting of C<sub>1s</sub> core level of the XPS data of GO (Fig. S4a) shows two components observed at 286.07 and 287.6 eV assigned to C–OH and/or C–O–C, and C=O, respectively. In the case of rGO (Fig. S4b), a marked reduction of the components associated with oxygenated functional groups occurred and an important increase on C=C at 285 eV was observed, which agrees with other analysis results (Raman, fluorescence spectra).

## 3.2 Optimizing the operating conditions

### 3.2.1 External current collectors and electrodes

In the present research, all systems used were compact systems made of neoprene rubber sheets, and a cation exchange membrane was used to separate both chambers. Various trials were carried out to investigate the optimum operating conditions, including external current collectors and

different anode and cathode electrodes, for the MFC's performance. Table S2 summarizes these experimental trails. Both voltage and current were monitored daily in all trails using a digital multimeter, and the results are shown in Fig. S5. It showed straight forward evidence of electricity generation (voltage reading) in all the experimental trials. In the experimental trial (I), a low-voltage reading was observed, which was concomitant with the breakdown of the copper wire connected to the cathode, resulting in the disconnecting of the cathode and the cessation of the experiment. This failure of copper wire connected to the cathode could have been a consequence of using sulfuric acid, which led to copper dissolution [43, 44]. Due to the corrosion of copper wire in the cathodic chamber, titanium wire was used as a substitute to connect the cathode, and an experimental trial (II) was carried out. The data obtained from experimental trial II displayed an enhancement in the voltage reading; however, another cut of the copper wire in the anode chamber occurred later. Cutting copper wire can be attributed to a microbial effect since the inoculum is mixed sludge, and some microorganisms may affect the rigidity of the wire and eventually lead to temporarily disconnecting the electrode. Microbial corrosion is a well-known phenomenon [14, 44]. To overcome the current disconnection, an experimental trial (III) was done, whereas titanium wires were used for current collection. In addition, carbon cloth supported on stainless steel mesh was used as electrodes on both poles. The obtained results were lower than those obtained in experimental trial II; additionally, corrosion of the stainless-steel mesh in the anodic chamber occurred [45, 46] (Fig. S6). No changes in titanium wires were observed, as titanium is known for its high resistance to corrosion, either microbial or chemical [46]. Based on the results of experimental trail (iii) (Fig. S6), the mixed sludge used in the present study is very sensitive to the presence of metals, and in fact, it can cause focal pitting. To overcome the drawbacks in experimental trial (iii), graphite

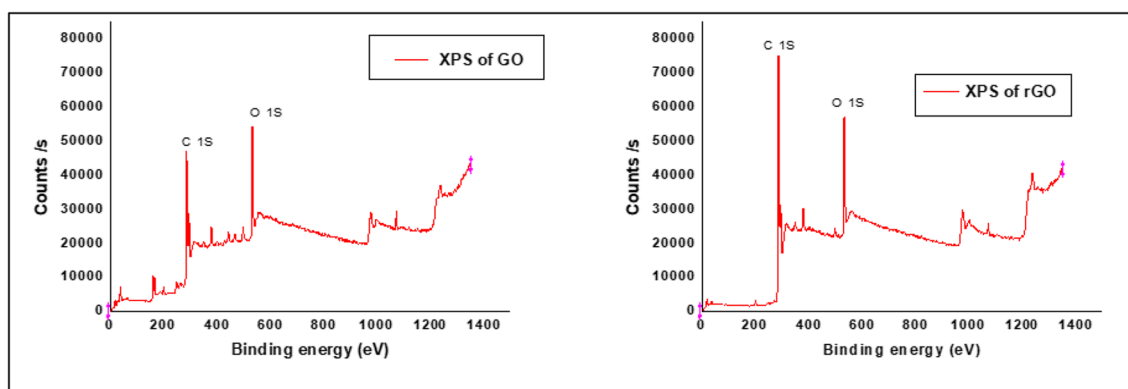


Fig. 5 The XPS spectra of GO (left) and rGO (right)



plate was used as an anode, and carbon cloth supported on stainless steel mesh was used as a cathode, with titanium wires as the current collector, representing experimental trial (iv). Results (Fig. S5) showed a more stable system without any interruptions, which was evidenced by a high voltage value without obvious fluctuations. In experimental trial (iv), the highest voltage reached 800 mV when the lowest resistance of 10 Ω was applied and after 20 days (about 3 weeks) of running the experiment. Accordingly, the configuration of using a compact system made of neoprene rubber with graphite plate as anode and carbon cloth supported on stainless steel mesh as cathode with titanium wires as current collector was evidently the best system that could be adapted for further experiments.

### 3.3 MFC performance with coated anode electrode

Based on the characterization of the prepared nanocarbonized materials, the graphite plate anode is coated with nanocarbonized material prepared at 500 °C (GO) and 700 °C (rGO). Table 2 lists the configuration of MFCs with coated and uncoated anodes.

Voltage was monitored daily for 15 days (about 2 weeks) of operation in all cells to estimate electricity generation; the

results are given in Fig. 6. Concerning cell potential, using a cell with a graphite plate coated with GO as an anode provides the highest voltage output (≈ 1000 mV), while the other two setup cells gave lower potential. This result confirms the higher electrogenic activity of the electrode and reaction rate in the anode chamber due to the highest surface area and high distribution of pore size. Interestingly, when rGO was used for coating, almost the same potential pattern was obtained as that GO-coated material but at a lower value. This indicated that carbonization temperature can affect the performance of coating materials and their electrical conductivity. This observation confirms the importance of our prepared nanocarbonized material for MFC performance. As confirmed by XPS data, the presence of function groups on the material surface improves bacteria growth on the electrode surface.

### 3.4 Electrochemical behavior of MFCs

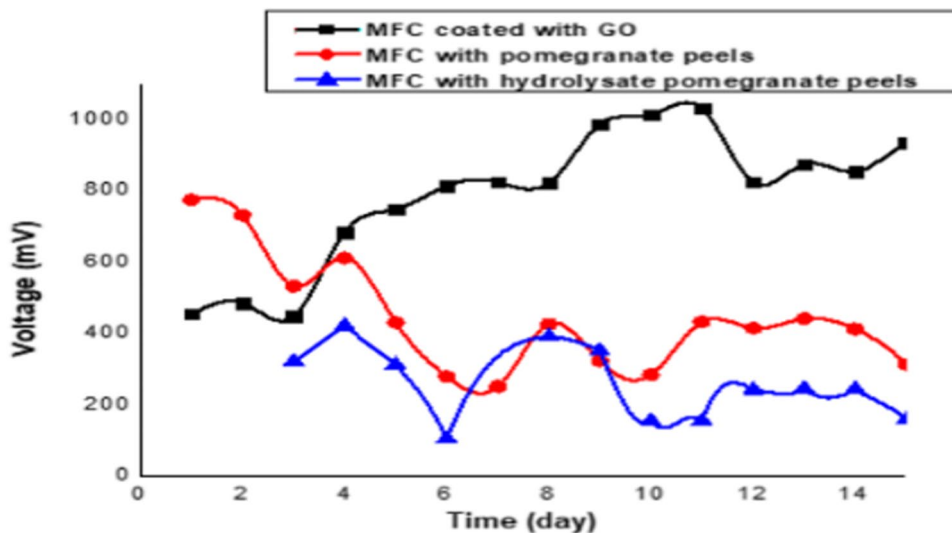
#### 3.4.1 Cyclic voltammetry

In this work, cyclic voltammetry was carried out at different scanning rates of 10, 25, 50, and 100 mV/s. The resulted cyclic voltammograms are presented in Figs. S7-8. From the voltammograms, we can conclude that high current is

**Table 2** Microbial fuel cells with different anode electrode materials

Cell	Non-coated MFC cell	Coated MFC cell with reduced graphene oxide carbonized at 700 °C	Coated MFC cell with graphene oxide carbonized at 500 °C
Anode	Graphite plates (7×1×0.5 cm)	Graphite plates (7×1×0.5cm) coated by rGO	Graphite plates (7×1×0.5cm) coated by GO
Cathode	Carbon cloth supported on stainless steel mesh (5 cm × 5cm)		
Current collector	Titanium wire (1mm diameter)		
Anolyte	Synthetic solution containing (per liter): 1 g acetate; NH <sub>4</sub> Cl, 0.15 g; NaCl,0.5 g; MgSO <sub>4</sub> , 0.015 g; CaCl <sub>2</sub> , 0.02 g; NaHCO <sub>3</sub> , 0.5 g; and trace element, 1 ml.		
Catholyte	100 mM potassium dichromate dissolved in 250 mM sulfuric acid		

**Fig. 6** Cell voltage generation during the operating period for noncoated and coated MFC

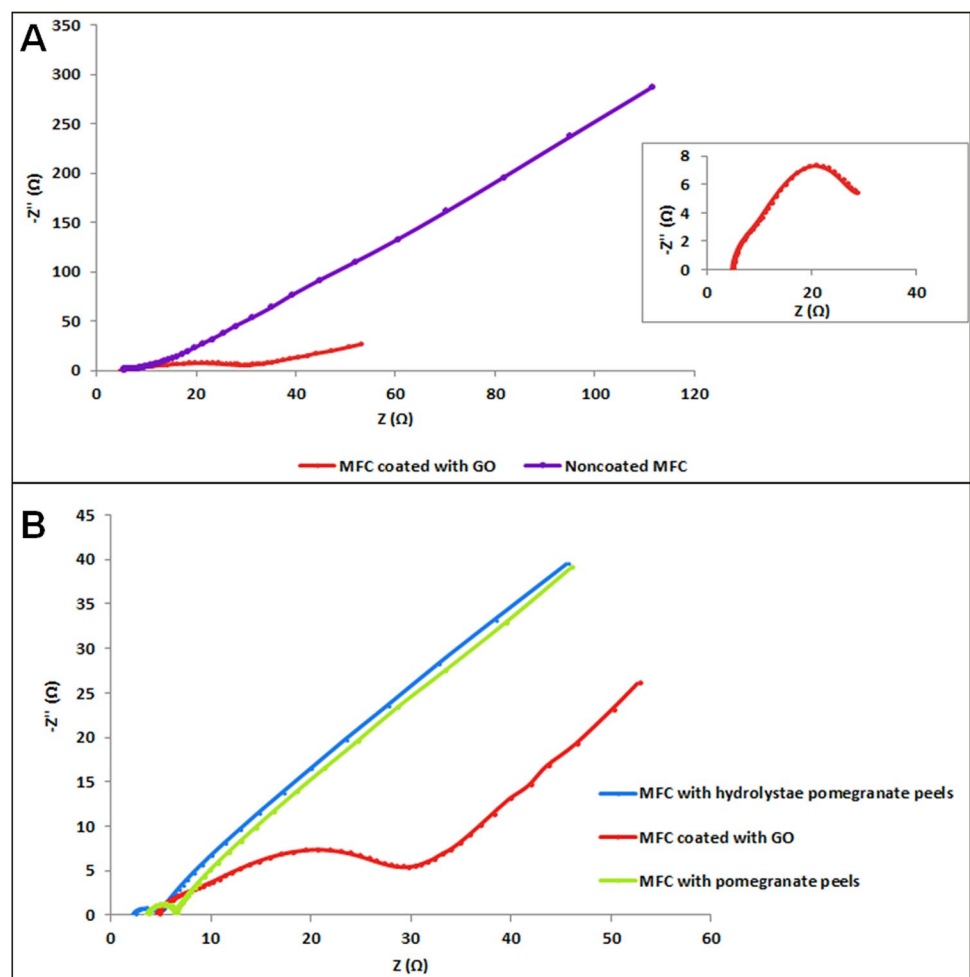


observed at faster scanning rates and a higher potential window of 100 mV/s compared to lower ones. The obtained results agree well with those reported in the literature [27], whereas faster scan rates lead to increased electron transfer, resulting in higher currents. The continuing increase of the peak currents with successive potential scans indicated the conductive anode surface area. At a lower scanning rate of 10 mV/s, a reduction peak is observed, indicating the reduction of dichromate at the cathode. The upper half of the curve indicated the oxidation potential, producing electrons that cause the generation of electric current, while the lower half depicted the reduction potential, consuming electrons and thus moving back to the initial voltage. This reduction peak is observed at lower scanning rates (10 mV/s and 25 mV/s) and eliminated at higher scanning rates, suggesting complete reduction of dichromate with a potential of 0.6–0.7 V and reaching steady state. This effect is known as the faradic effect; this effect does not appear on other MFC. The cyclic voltammograms of the MFCs have many differences that may be due to using various electrode materials, applying different sweep potentials, organic substrates, and the conductivity of the anode liquor applied in this work.

### 3.4.2 Electrical impedance spectroscopy

Electrical impedance spectroscopy (EIS) is a useful tool for figuring out the electrochemical characteristics of an MFC's anode and cathode. The internal resistance ( $R_s$ ) of MFC is divided into several types: charge transfer resistance is related to high frequencies and represented by the diameter of the semicircle in the Nyquist plot, and the straight line at low frequencies represents the diffusive resistance of the electrolyte in the electrode that hinders the transfer of charges from solution to electrode [47]. The lower values of  $R_s$  may improve the total conductivity through the whole MFC cell and could also be considered a reflection of the high rate of electron transfer between the anode and the cathode. Figure 7 A shows the electrical impedance of MFCs, recorded in the frequency range of 0.01 Hz–100 kHz. The noncoated MFC has a high diffusive resistance value that is exhibited at low frequencies, representing slow bio-electrochemical substrate oxidation-reduction processes, in contrast to the MFC with an anode coating with GO, which showed lower diffusive resistance, indicating higher oxidation-reduction processes. These results agreed well

**Fig. 7** Electrochemical impedance spectroscopy of **A** coated and noncoated MFC and **B** different MFC setups (in the presence of pomegranate peels, hydrolyzed pomegranate peels, and anodes coated with GO)



with cyclic voltammetry data and Nyquist diameter (charge transfer resistance) = 27; thus, this anode in an MFC cell can act as a capacitor (specific capacitance = 0.835 F/g). This charge transfer resistance was measured under different external resistances in the range of 10 to 1000.

### 3.5 Comparison between MFC performance of pomegranate peels, hydrolysate pomegranate peels, and coated anode electrode with GO

The purpose of estimating the advantages of coating the anode with the prepared nanocarbonized material GO rather than using pomegranate peels directly or using pomegranate peel hydrolysate as carbon sources on MFC performance and cell potential along with electrical current monitoring for 15 days (about 2 weeks) is applied and represented in Fig. 8a–b for all MFCs used. The observed results indicated that the highest electric potential is produced from cells with an anode coated with GO compared to the other cells. The electricity potential value was gradually increased from day 1 to day 11 for this cell; however, lower patterns were observed for other cells due to the high surface area of the coated anode and the presence

of micropores in the coated GO that improve the extracellular electron transfer process. These fluctuations in electrical potential generated may be influenced by the condition and community development of the microorganisms in the MFC reactor. Moreover, these observations can be closely related to the substrates used, whether they are easy or difficult to degrade, and differ in the growth capability of microorganisms MFC [48]. This study used electrochemical impedance spectroscopy to assess the internal resistance of various MFCs over the frequency range of 0.01 Hz to 100 kHz. The results are depicted in Fig. 7B. It is clearly seen that the coated electrode with GO showed lower diffusive resistance, indicating higher oxidation reduction processes in MFC, which was confirmed by cyclic voltammetry measurements. In addition, the large Nyquist diameter of 27 Ω as compared to other cells of 4 Ω confirms that the charge resistance of this cell can act as a capacitor. In addition, the starting points of the curves were remarkably similar, indicating similar  $R_s$  values for all MFCs.

Table 3 summarizes comparisons between different microbial fuel cells used in this study concerning electricity generation. The resulted data showed that cells with a graphite plate coated with GO in the presence of acetate substrate gave the highest power density of 12.46 W/m<sup>2</sup> after 15 days

**Fig. 8** a Cell voltage monitoring. b Electrical response of different MFC setups (in presence of pomegranate peels, hydrolysate pomegranate peels and anode coated by nanocarbonized material)

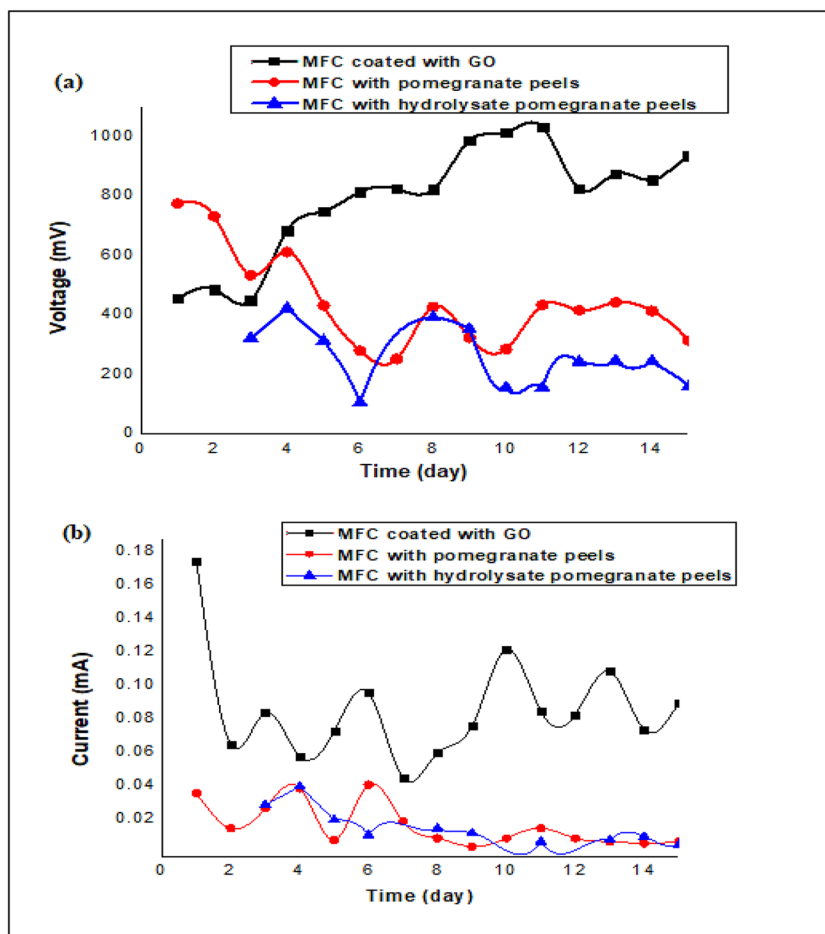


**Table 3** Power density comparison between different MFCs

System	Power density (W/m <sup>2</sup> )	% power density over control cell
Control cell: cell with free graphite plate as anode along with acetate as substrate	4.37	100
Cell with anode coated with GO along with acetate as substrate	12.46	285 (2.85-fold increase)
Cell with free graphite plate as anode along with pomegranate peels as substrate	1.85	42.33
Cell with free graphite plate as anode along with pomegranate peels hydrolysate as substrate	0.035	0.8

(about 2 weeks) of incubation, while cells with a free graphite plate with pomegranate peel hydrolysate gave the lowest value of 0.035 W/m<sup>2</sup>. The higher value of power density in the presence of GO as coating anode material is due to the larger pores of the anode which encourage extracellular electron transfer. Lower values of power density in the presence of hydrolysate may be due to the presence of some phenolic compounds and/or other components in hydrolysate that could inhibit microbial growth in the anode chamber and reduce microbial fuel cell performance. The obtained results agree with previous reports about microbial hydrolysis of lignocellulosic biomass [49, 50] and antimicrobial activity of pomegranate peel extract [51]. When pomegranate peels were used directly as substrate for anaerobic digestion in an anode chamber, the resultant power density was lower than that obtained using acetate as substrate because pomegranate peels are a complicated compound with an exceedingly high carbon to nitrogen ratio, and for anaerobic degradation, we must adjust the carbon to nitrogen ratio, which is one of the main factors affecting anaerobic microbial growth. Accordingly, direct use of pomegranate peels as substrate is not good for this process unless we add other chemicals that will adjust the carbon-to-nitrogen ratio. This finding agrees with previous reports [50, 52, 53]. We can conclude that using graphite plates coated with GO as anodes gave the best performance for our constructed microbial fuel cell system in the presence of acetate as substrate.

## 4 Conclusion

A dual-chamber MFC was fabricated with optimized operating conditions for electricity generation. Nanocarbonized materials were prepared from pomegranate peels at different temperatures (300, 500, and 700 °C) in the presence of ferrocene to be tested as a coating anode material to enhance the performance of the fabricated MFC. The nano-sized materials were fully characterized, and electrochemical characterization of the MFC was performed. Results revealed that the anode coated with nanocarbonized material prepared at 500 °C illustrated the best MFC performance, yielding high power density, low diffusive resistance by improving the

extracellular electron transfer process, and charge transfer resistance, demonstrating the anode as a capacitor. Lowering the cost of MFC anode materials by using high-performance biomass waste is crucial for our future use of MFCs in real-world applications. These encouraging results make the green nano-graphene oxide (green nano-carbonized material) made from pomegranate peels appropriate for use as an appealing covering anode on MFC in a variety of applications, particularly for water and wastewater treatment.

**Supplementary Information** The online version contains supplementary material available at <https://doi.org/10.1007/s13399-023-04964-6>.

**Author contributions** Afaf Abdel Razik: conceptualization; methodology; investigation; writing—original draft; writing—review and editing. Ali El-Dissouky: supervision, investigation, writing—review and editing. Mohammed Salah El-Din Hassouna: supervision, writing—review and editing. Amel F. Elhusseiny: conceptualization, supervision, writing—review and editing. Abd El-Hady B. Kashyout: visualization, data analysis, writing—review and editing. Zhen He: writing—review and editing; funding acquisition. Hanan Moustafa: conceptualization; methodology; writing—original draft; writing—review and editing; supervision; project administration; funding acquisition.

**Funding** Open access funding provided by The Science, Technology & Innovation Funding Authority (STDF) in cooperation with The Egyptian Knowledge Bank (EKB). This work was financially supported by STDF joint fund project between Alexandria University, Egypt, and Washington University in St. Louis USA. STDF project ID# 42697, cycle 19.

**Data availability** The datasets used and/or analyzed during the current study are available from the corresponding author upon reasonable request.

## Declarations

**Ethics approval and consent to participate** Not applicable.

**Consent for publication** All authors approved the consent for publishing the manuscript to biomass conversion and biorefinery.

**Competing interests** The authors declare no competing interests.

**Open Access** This article is licensed under a Creative Commons Attribution 4.0 International License, which permits use, sharing, adaptation, distribution and reproduction in any medium or format, as long as you give appropriate credit to the original author(s) and the source, provide a link to the Creative Commons licence, and indicate if changes were made. The images or other third party material in this article are

included in the article's Creative Commons licence, unless indicated otherwise in a credit line to the material. If material is not included in the article's Creative Commons licence and your intended use is not permitted by statutory regulation or exceeds the permitted use, you will need to obtain permission directly from the copyright holder. To view a copy of this licence, visit <http://creativecommons.org/licenses/by/4.0/>.

## References

- Logan BE, Rabaey K (2012) Conversion of wastes into bioelectricity and chemicals by using microbial electrochemical technologies. *Science* 337(6095):686–690
- Li S, Chen G, Anandhi A (2018) Applications of emerging bioelectrochemical technologies in agricultural systems: a current review. *Energies* 11(11):2951
- Liu F, Moustafa H, Hassouna MSE-D, He Z (2020) Resource recovery from wastewater can be an application niche of microbial desalination cells. *Environ Int* 142:105855
- Liu F, Worland A, Tang Y, Moustafa H, Hassouna MSE-D, He Z (2022) Microbial electrochemical ammonia recovery from anaerobic digester centrate and subsequent application to fertilize *Arabidopsis thaliana*. *Water Res* 220:118667
- Li T, Li R, Zhou Q (2021) The application and progress of bioelectrochemical systems (BESs) in soil remediation: a review. *Green Energy Env* 6(1):50–65
- Feng H, Ge Z, Chen W, Wang J, Shen D, Jia Y, Qiao H, Ying X, Zhang X, Wang M (2018) Carbonized cow dung as a high performance and low cost anode material for bioelectrochemical systems. *Front Microbiol* 9:2760
- Rao N, Singh R, Bashambu L (2021) Carbon-based nanomaterials: synthesis and prospective applications. *Mater Today: Proc* 44:608–614
- Mahmoud RH, Samhan FA, Ibrahim MK, Ali GH, Hassan RY (2021) Formation of electroactive biofilms derived by nanostructured anodes surfaces. *Bioprocess Biosyst Eng* 44:759–768
- Mahanta V, Raja M, Kothandaraman R (2019) Activated carbon from sugarcane bagasse as a potential positive electrode catalyst for vanadium redox flow battery. *Mater Lett* 247:63–66
- Gómez-Urbano JL, Moreno-Fernández G, Arnaiz M, Ajuria J, Rojo T, Carriazo D (2020) Graphene-coffee waste derived carbon composites as electrodes for optimized lithium ion capacitors. *Carbon* 162:273–282
- Dhand V, Yadav M, Kim SH, Rhee KY (2021) A comprehensive review on the prospects of multi-functional carbon nano onions as an effective, high-performance energy storage material. *Carbon* 175:534–575
- Taer E, Taslim R, Putri A, Apriwandi A, Agustino A (2018) Activated carbon electrode made from coconut husk waste for supercapacitor application. *Int J Electrochem Sci* 13(12):12072–12084
- Dwivedi KA, Huang S-J, Wang C-T, Kumar S (2022) Fundamental understanding of microbial fuel cell technology: recent development and challenges. *Chemosphere* 288:132446
- Zhu X, Logan BE (2014) Copper anode corrosion affects power generation in microbial fuel cells. *J Chem Technol Biotechnol* 89(3):471–474
- Zhu K, Xu Y, Yang X, Fu W, Dang W, Yuan J, Wang Z (2022) Sludge derived carbon modified anode in microbial fuel cell for performance improvement and microbial community dynamics. *Membranes* 12(2):120
- Kumari A, Dora J, Kumar A, Kumar A (2012) Pomegranate (*Punica granatum*)—overview. *Int J Pharm Chem Sci* 1(4):1218–1222
- Asnawi M, Azhari S, Hamidon MN, Ismail I, Helina I (2018) Synthesis of carbon nanomaterials from rice husk via microwave oven. *J Nanomater* 2018:1–5
- Elessawy NA, El Nady J, Wazeer W, Kashyout A (2019) Development of high-performance supercapacitor based on a novel controllable green synthesis for 3D nitrogen doped graphene. *Sci Rep* 9(1):1129
- Moustafa E, El Nady J, Kashyout AE-HB, Shoueir K, El-Kemary M (2021) Fabrication of high yield photoluminescent quantized graphene nanodiscs for supercapacitor devices. *ACS omega* 6(36):23090–23099
- Al-Qodah Z, Shawabkah R (2009) Production and characterization of granular activated carbon from activated sludge. *Braz J Chem Eng* 26:127–136
- Saleem A, Hussain A, Chaudhary A, Ahmad Q-U-A, Iqtedar M, Javid A, Akram AM (2020) Acid hydrolysis optimization of pomegranate peels waste using response surface methodology for ethanol production. *Biomass Convers Biorefin* 12:1513–15241
- Versaci D, Nasi R, Zubair U, Amici J, Sgroi M, Dumitrescu M, Francia C, Bodoardo S, Penazzi N (2017) New eco-friendly low-cost binders for Li-ion anodes. *J Solid State Electrochem* 21:3429–3435
- Elgrishi N, Rountree KJ, McCarthy BD, Rountree ES, Eisenhart TT, Dempsey JL (2018) A practical beginner's guide to cyclic voltammetry. *J Chem Educ* 95(2):197–206
- Pandit S, Sengupta A, Kale S, Das D (2011) Performance of electron acceptors in catholyte of a two-chambered microbial fuel cell using anion exchange membrane. *Bioresour Technol* 102(3):2736–2744
- Rismani-Yazdi H, Carver SM, Christy AD, Tuovinen OH (2008) Cathodic limitations in microbial fuel cells: an overview. *J Power Sources* 180(2):683–694
- You S, Zhao Q, Zhang J, Jiang J, Zhao S (2006) A microbial fuel cell using permanganate as the cathodic electron acceptor. *J Power Sources* 162(2):1409–1415
- Bard AJ, Faulkner LR (2001) Fundamentals and applications. *Electrochem Methods* 2(482):580–632
- Savéant J-M (2006) Elements of molecular and biomolecular electrochemistry: an electrochemical approach to electron transfer chemistry. John Wiley & Sons
- Zhou J, Guo S (2021) Carbon-based anode materials for potassium-ion batteries: From material, mechanism to performance. *SmartMat* 2(2):176–201
- Saadi W, Souissi SN, Ouederni A (2016) Pomegranate peels precursor used in the synthesis of activated carbon: application in the wastewater treatment. *J Int Environ App Sci* 11(4):118–230
- Salih SI, Oleiwi JK, Mohamed AS (2018) Investigation of mechanical properties of PMMA composite reinforced with different types of natural powders. *ARNP J Eng App Sci* 13(22):8889–8900
- Aziz M, Halim FA, Jaafar J (2014a) Preparation and characterization of graphene membrane electrode assembly. *J tekno* 69(9):11–14
- Jorio A, Ferreira EHM, Moutinho MV, Stavale F, Achete CA, Capaz RB (2010) Measuring disorder in graphene with the G and D bands. *physica status solidi (b)* 247(11–12):2980–2982
- Uskoković V (2021) A historical review of glassy carbon: synthesis, structure, properties and applications. *Carbon Trends* 5:100116
- Aziz M, Halim FSA, Jaafar J (2014b) Preparation and characterization of graphene membrane electrode assembly. *J Tekno* 69(9):11–14
- Wu J-B, Lin M-L, Cong X, Liu H-N, Tan P-H (2018) Raman spectroscopy of graphene-based materials and its applications in related devices. *Chem Soc Rev* 47(5):1822–1873
- Schüpfer DB, Badaczewski F, Peilstöcker J, Guerra-Castro JM, Shim H, Firoozabadi S, Beyer A, Volz K, Presser V, Heiliger C (2021) Monitoring the thermally induced transition

- from sp<sup>3</sup>-hybridized into sp<sup>2</sup>-hybridized carbons. Carbon 172:214–227
38. Georgakilas V, Otyepka M, Bourlinos AB, Chandra V, Kim N, Kemp KC, Hobza P, Zboril R, Kim KS (2012) Functionalization of graphene: covalent and non-covalent approaches, derivatives and applications. Chem Rev 112(11):6156–6214
  39. Tawfik A, Azzam AM, El-Dissouky A, Ibrahim AY, Nasr M (2023) Synergistic effects of paper mill sludge and sulfonated graphene catalyst for maximizing bio-hydrogen harvesting from sugarcane bagasse de-polymerization. J Environ Manag 326:116724
  40. Sharma N, Arif M, Monga S, Shkir M, Mishra YK, Singh A (2020) Investigation of bandgap alteration in graphene oxide with different reduction routes. Appl Surf Sci 513:145396
  41. Shahriary L, Athawale AA (2014) Graphene oxide synthesized by using modified hummers approach. Int J Renew Energy Environ Eng 2(01):58–63
  42. Kang M-A, Ji S, Kim S, Park C-Y, Myung S, Song W, Lee SS, Lim J, An K-S (2018) Highly sensitive and wearable gas sensors consisting of chemically functionalized graphene oxide assembled on cotton yarn. RSC Adv 8(22):11991–11996
  43. Thaçi VHR, Berisha A, Bogdanov J (2020) Corrosion study of copper in aqueous sulfuric acid solution in the presence of (2E, 5E)-2, 5-dibenzylidenecyclopentanone and (2E, 5E)-bis [(4-dimethylamino) benzylidene] cyclopentanone: experimental and theoretical study. Open Chem 18(1):1412–1420
  44. Brusic V, Eldridge MAFBN, Novak FP, Kaufman FB, Rush BM, Frankel GS (1991) Copper corrosion with and without inhibitors. J Electrochem Soc 138(8):2253–2259
  45. CA L (2017) Microbiological corrosion: mechanism, control and impact—a review. Int J Adv Manuf Technol 92:4241–4252
  46. Amendola R, Acharjee A (2022) Microbiologically influenced corrosion of copper and its alloys in anaerobic aqueous environments: A review 2022. Front Microbiol 13
  47. Villano M, Aulenta F, Ciucci C, Ferri T, Giuliano A, Majone M (2010) Bioelectrochemical reduction of CO<sub>2</sub> to CH<sub>4</sub> via direct and indirect extracellular electron transfer by a hydrogenophilic methanogenic culture. Bioresource Tech 101:3085–3090
  48. Bhardwaj S, Yadav P, Ghosh S, Basu T, Mahapatro A (2016) Biosensing test bed using electrochemically deposited reduced graphene oxide. ACS Appl Mater Inter 8(37):24350–24360
  49. Menzel T, Neubauer P, Junne S (2020) Role of microbial hydrolysis in anaerobic digestion. Energies (Basel) 13:1–29
  50. Tsegaye B, Balomajumder C, Roy P (2019) Microbial delignification, and hydrolysis of lignocellulosic biomass to enhance biofuel production: an overview and future prospect. Bull Natl Res Cent 43(51):1–16
  51. Al-Zoreky (2009) Antimicrobial activity of pomegranate (*Punica granatum* L.) fruit peels. Int J Food Microbiol 134:244–248
  52. El Barnossi A, Moussaid F, Iraqi Housseini A (2021) Tangerine, banana, and pomegranate peels valorisation for sustainable environment: a review. Biotechnol Rep 29:e00574
  53. Poltronieri OD (2016) Organic recycling of agricultural waste today: composting and anaerobic digestion. Biotransformation Agric Waste By-Products Food, Feed Fibre Fuel 69:69–124

**Publisher's Note** Springer Nature remains neutral with regard to jurisdictional claims in published maps and institutional affiliations.